Supplement of

Satellite soil moisture data assimilation impacts on modeling weather and ozone in the southeastern US - part I: an overview

Huang et al.

Correspondence to: Min Huang (mhuang10@gmu.edu)

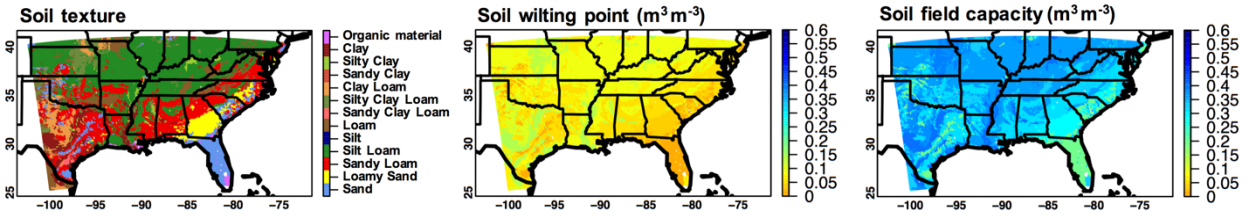

Figure S1. Grid-dominant (left) soil texture types; (middle) soil wilting point; and (right) soil field capacity used in the 12 km LIS/WRF-Chem simulations. The soil wilting points and field capacities are determined from the soil texture types and a soil parameter lookup table.

In the Jarvis-type of parameterizations, a soil moisture (SM) limitation factor f_{sm}^{-1} ($f_{sm} = \min\left[1, \max\left(f_{min}, \frac{\text{SM} - \text{Wilting point}}{\text{Field capacity} - \text{Wilting point}}\right)\right]$, where f_{min} is slightly above 0), which ranges from f_{min} (dry) to 1 (wet), is used to adjust the stomatal resistance in the Noah land surface model. This type of adjustment to the modeled stomatal resistance has also been applied to deposition calculations in chemical transport models (e.g., Anav et al., 2018). f_{sm} is calculated based on SM from a given soil layer between the surface and the root zone which depends on land use/cover (LULC), and alternatively, it can be based on the maximum or column-averaged SM within these soil layers. Including such a SM limitation factor may not necessarily improve the modeled stomatal resistance or/and deposition velocity partially due to the uncertainty in the model's LULC input and the prescribed constant values in these algorithms.

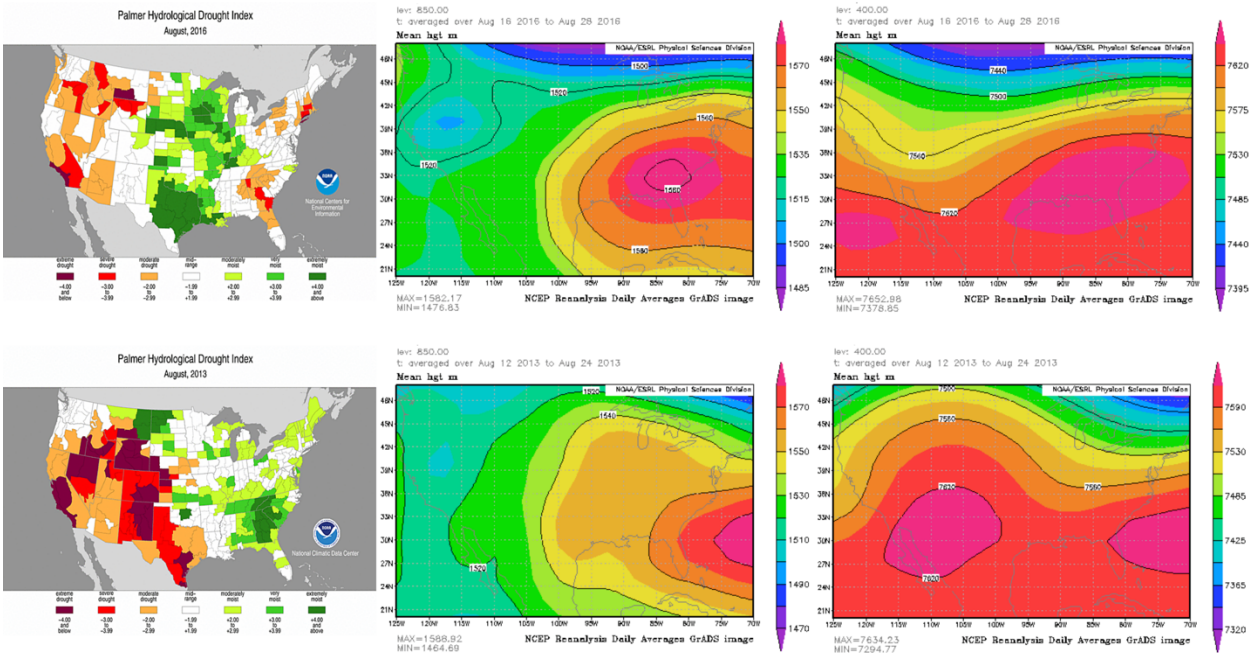

Figure S2. Drought and synoptic conditions in August 2016 and August 2013: (left) Palmer Hydrological Drought Index in August 2016 and August 2013; (middle) 850 hPa geopotential heights during 16-28 August 2016 and 12-24 August 2013; and (right) 400 hPa geopotential heights during 16-28 August 2016 and 12-24 August 2013. Data sources: National Climatic Data Center for the drought index and NCEP/NCAR reanalysis for geopotential heights.

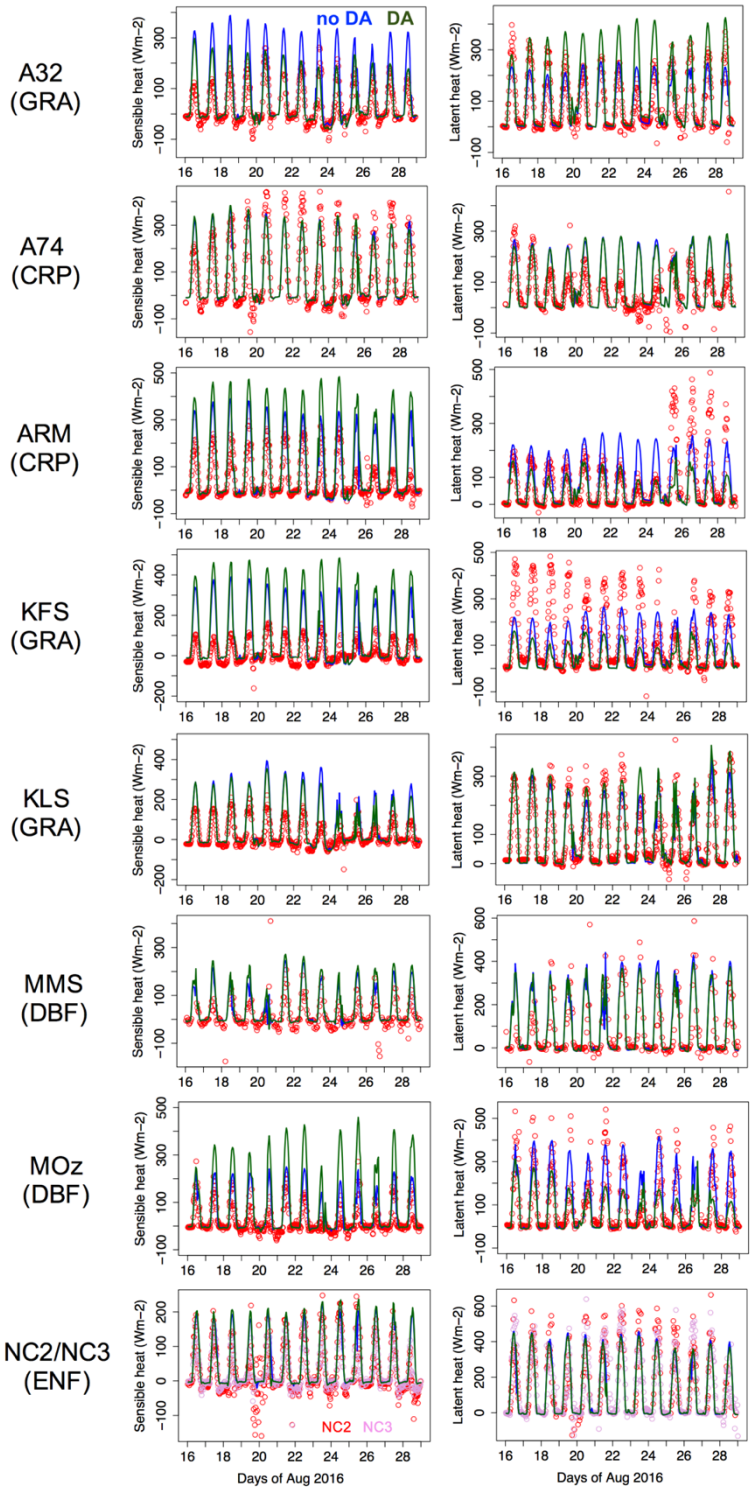

Figure S3. Evaluation of WRF-Chem modeled (left) sensible and (right) latent heat fluxes at selected FLUXNET sites shown in Figure 5b. Observations, base case and the "assim" case results are shown in red/pink open circles, blue and green solid lines, respectively. Acronyms of the land cover classifications of these sites are included in parentheses below the site names: GRA: grassland; CRP: cropland; DBF: deciduous broadleaf forests; ENF: evergreen needleleaf forests. Observation frequency is hourly at MMS and half-hourly at the other sites.

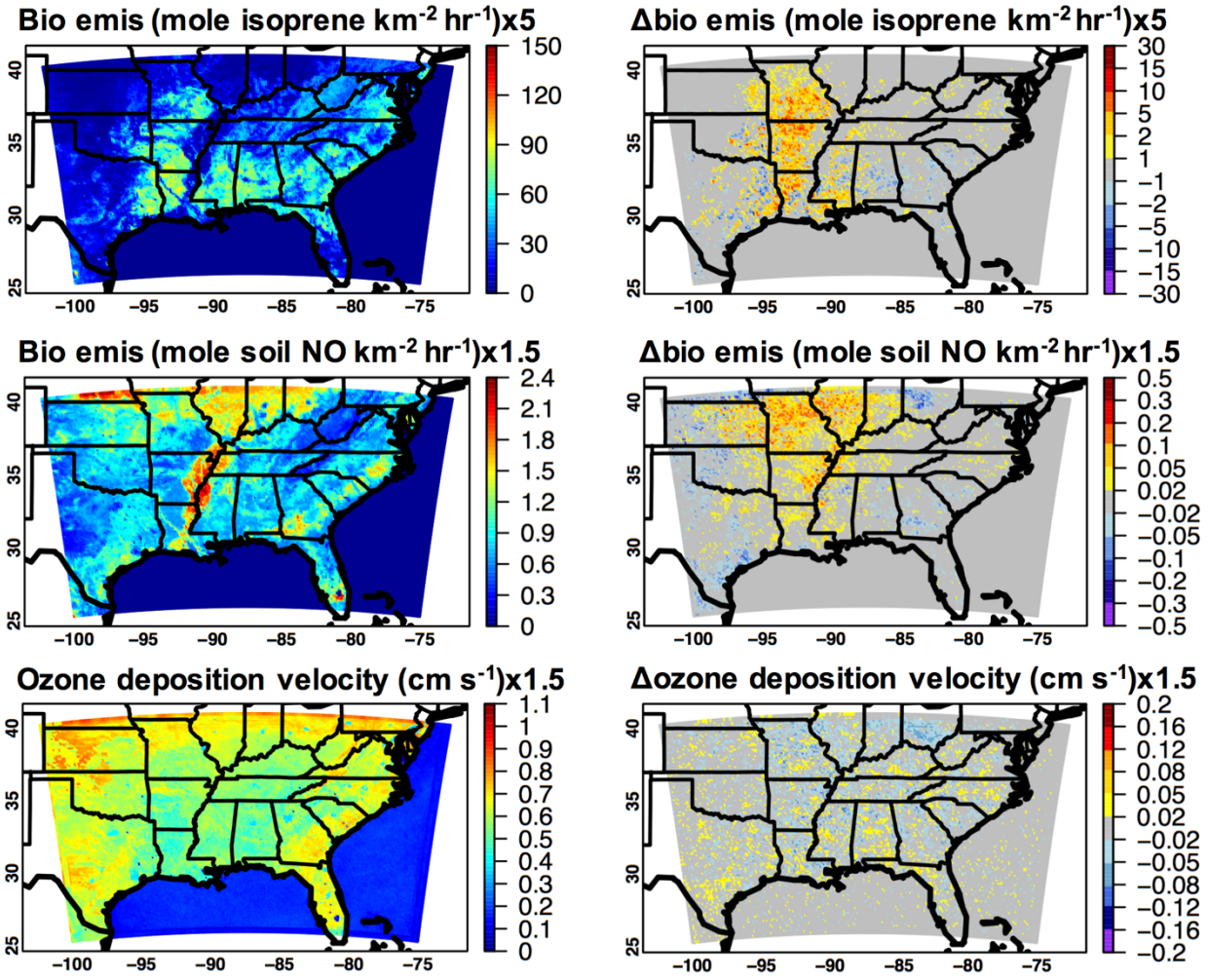

Figure S4. Period-mean (16-28 August 2016) WRF-Chem early morning (12 UTC)/evening (00 UTC) biogenic emissions of (upper) isoprene and (middle) soil NO; and (lower) O_3 deposition velocity. The left panels are the base case results, and the SMAP DA impacts on these model fields are shown in the right panels. Results shown here and in Figure 3k-p indicate strong diurnal cycles in the WRF-Chem modeled biogenic emissions and O_3 deposition velocities as well as their responses to the SMAP DA.

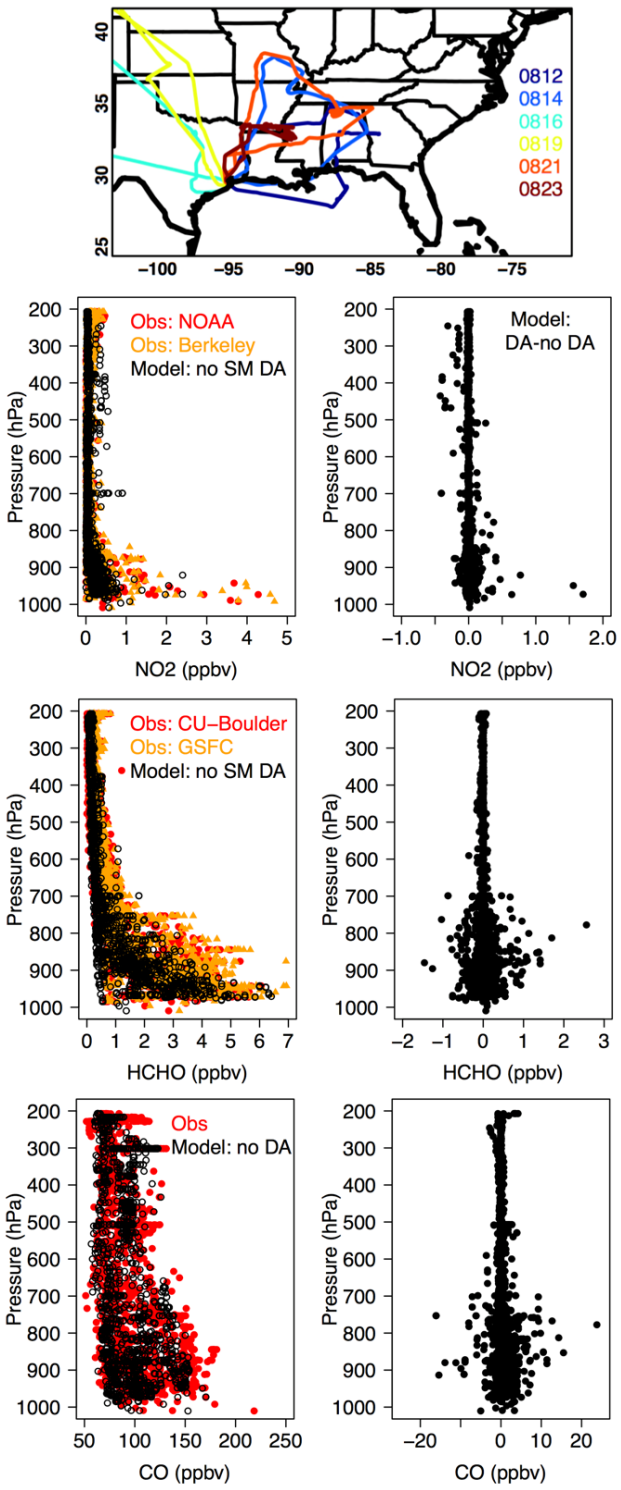

Figure S5. Evaluation of WRF-Chem modeled NO_2, HCHO, and CO with the DC-8 aircraft observations during six SEAC^{4}RS flights in August 2013. The top panel shows the related fight paths. The other panels present 1-minute averaged observations along with their WRF-Chem counterparts from the "SEACf" case and the differences between the "SEACa" and "SEACf" cases.